energies

MDPI

Article

Adaptive Backstepping Control with Online Parameter Estimator for a Plug-and-Play Parallel Converter System in a Power Switcher

Chujia Guo [1], Aimin Zhang [1,*], Hang Zhang [2] and Lei Zhang [3]

[1] School of Electronic and Information Engineering, Xi'an Jiaotong University, No. 28, West Xianning Road, Xi'an 710049, China; a360922608@163.com
[2] School of Electrical Engineering, Xi'an Jiaotong University, No. 28, West Xianning Road, Xi'an 710049, China; zhangh@mail.xjtu.edu.cn
[3] School of Electronics and Information, Xi'an Polytechnic University, No. 19, South Jinhua Road, Xi'an 710049, China; carol1208@163.com
* Correspondence: zhangam@mail.xjtu.edu.cn; Tel.: +86-29-8266-8665 (ext. 167)

Received: 13 November 2018; Accepted: 17 December 2018; Published: 18 December 2018

Abstract: This study aims to address the inherent uncertainty in plug loads and load extraction, distributed generation, and the inevitable circulating current in a parallel structure. Therefore, in this paper, an adaptive backstepping control scheme with an online parameter estimator (OPE) for a plug-and-play parallel converter system in a four-port power switcher is proposed. The adaptive backstepping control method was designed in the dq0 coordinate system to suppress the circulating current in the zero-component; the circulating current can be suppressed by using an embedded algorithm and omitting the extra controller. An adaptive update law was designed to weaken the influence of the arbitrary plug and extraction operations in the DC and AC buses to realize the plug-and-play function. The transient tracking performance is governed by the limitation of maximum total errors in the voltage and current. As a result, the settling times of the voltage, current, and power decreased. Additionally, to further improve the system robustness, an online inductance and resistance estimator was established using an optimal algorithm that solves the weighted least squares problem. In the estimator, there are no additional voltage and current sensors needed, and the mean squared error (MSE) of the estimation can be minimized. Simulation studies on a two-converter parallel system with a plug-and-play function were conducted using MATLAB/SIMULINK (R2018b, MathWorks, Natick, MA, USA) to verify the effectiveness of the proposed adaptive backstepping control strategy. The results show that this strategy improves system performance over that of a system with unbalanced parameters among a parallel structure with AC and DC system disturbances caused by arbitrary plug and extraction operations.

Keywords: power switcher; parallel structure; circulation current; backstepping control; Lyapunov function; weighted least squares (WLS)

1. Introduction

Grid-tied distributed generation, microgrids, and variable loads are increasingly being utilized for power distribution. A key requirement for a distribution grid is a flexible connection mode [1–3]. In a hybrid AC/DC distribution grid, not only can a power switcher realize voltage isolation and voltage class conversion, it can also satisfy the flexible power supply requirements for medium- and low-voltage AC/DC loads. Consequently, the power switcher requires multi-voltage levels and connected ports to meet different electrical power demands. As a result, the multi-port power switcher has become an attractive device for use with a smart distribution grid to guarantee power quality,

realize multidirectional power flow control, and offer energy management services [4]. A distribution grid system connected by a four-port power switcher is shown in Figure 1. It can be seen that micro-photovoltaic generation plants, micro-energy storage systems, micro-wind turbines, and so on, are connected to the low-voltage DC and AC power system. Therefore, a plug-and-play functionality needs to be considered for governing the unpredictability of plug loads, load extraction, and distributed generation. To this end, the parallel structure of a low-voltage DC/AC converter system is gaining increasing attention [5–7], as it combines the functions of both energy conversion and the ability to govern arbitrary changes in loads and distributed generation. Furthermore, the rated power of the converter system can only increase or decrease by changing the number of paralleled converters. Owing to these features, low-voltage DC/AC converters with a parallel structure for distributed generation have been attracting increasingly more interest in recent years.

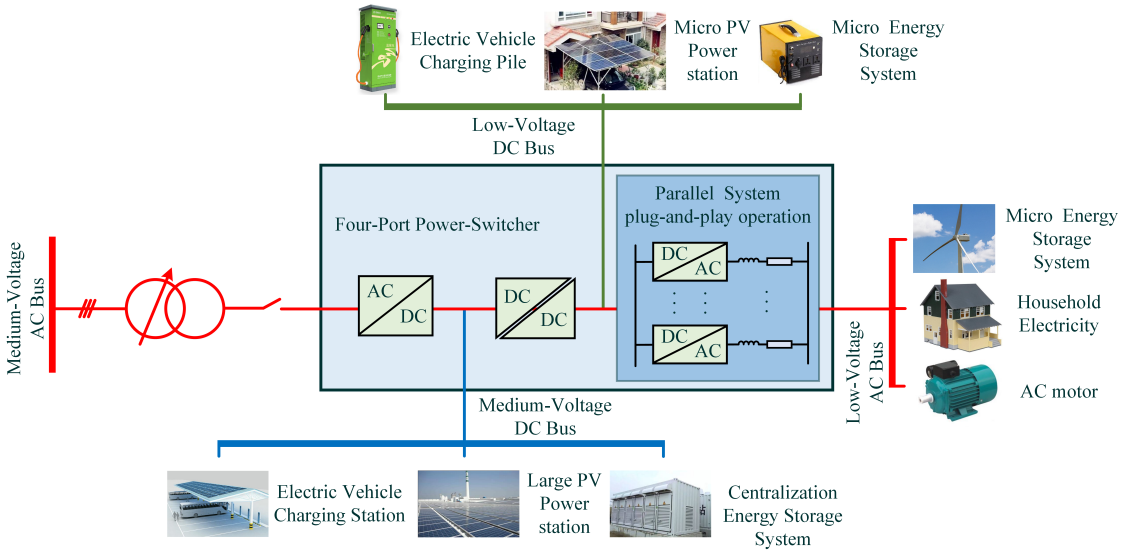

Figure 1. Power network system connected by a four-port power switcher.

However, two main challenges arise with the use of a plug-and-play parallel converter system in a four-port power switcher: (i) the transient performance is affected by unknown disturbances and arbitrary plug loads, load extraction, and distributed generation in both the AC and DC systems; (ii) the inevitable circulating current in the parallel structure reduces the rated transmission power and may damage the switching devices. Numerous studies have been conducted on this topic, where the goal is to achieve adaptive control of unknown dynamic or circulating current suppression for a paralleled structure.

To alleviate the problems created by disturbances from the variation in loads and distributed generation, often occurring in a plug-and-play situation, active disturbance rejection control (ADRC) is an attractive solution that has been previously applied [8]. Generally, ADRC is realized by using an extended state observer (ESO) to estimate all the disturbances and unknown dynamic processes [9,10]. In Ref. [11,12], ADRC with an ESO was proposed for a grid-connected inverter and a multi-timescale DC microgrid, respectively. In Ref. [13], ESO-based sliding mode control was proposed for a DC/DC buck converter. However, the parameters of the ESO needed to be reset when the disturbances changed violently; otherwise, the performance decreased drastically [14]. In order to obtain satisfactory performance in such a situation, the parameters of the ESO need to be tuned in real time. Although the gain of an ESO was able to be tuned automatically by using an adaptive extended state observer (AESO) to counteract the sensor noise in [15], the change in the unknown bounded disturbances was not considered. Further, an ESO is often used for disturbances with known probability distributions.

Moreover, while the stability of the estimation error dynamics of an ESO is easily determined [16,17], the stability of the whole control process has been rarely examined.

Owing to its excellent dynamic performance, model predictive control (MPC) is an attractive option for the control of power converters with arbitrary plug and extraction processes [18–20]. In Ref. [21], the implementation of an MPC-based current control strategy was implemented for different converters, and it resulted in better transient performance. In Ref. [22], an MPC-based voltage control strategy was designed for DC/DC converters to improve the dynamic performance. In Ref. [23], a prediction approach for set point automatic adjustment with a correction-enabled algorithm was applied to mitigate possible transients. Although MPC can regulate the process with few issues theoretically, it suffers from a stability problem due to model parameter mismatches. A mathematical analysis of the prediction error with uncertain model parameters was proposed in [24] to deal with model parameter mismatch, and an optimal nonlinear MPC was proposed in [25] to manage the modeling uncertainties and external disturbances. Although MPC leads to better transient performance, it comes with a high computational burden, which results in an inefficient programming process, especially for a parallel structure. Furthermore, MPC does not employ a modulation stage, which results in an unfixed switching frequency, and it is difficult to design the output filter. In addition, the stability of the control system is hard to guarantee with some widely-used algorithms.

Many methods have been studied to suppress circulating currents in the context of parallel power converter control. In Ref. [26,27], the AC component was isolated by a multi-winding transformer, and additional power sources were used to cut off the path of the circulating currents. Thus, the cost and weight increase with the use of these passive methods due to the extra hardware circuits required. Improved modulation techniques are commonly-used active methods [28]. The voltage zero vector of space-vector-pulse-width modulation (SVPWM) is used in each paralleled module to suppress the circulating current [29,30]. However, the control performance deteriorates when the system parameters are different in each converter module. A virtual impedance control method was proposed for current sharing and circulating current suppression [31,32]. However, these studies did not consider the mismatch of system impedance, which causes circulating currents to increase directly. In Ref. [33,34], an adaptive virtual impedance method was proposed to design the proper virtual impedance. Thus, the output current was limited by the virtual impedance. On the one hand, if a large virtual impedance is adopted, the rated output power capability decreases; on the other hand, if a small virtual impedance is adopted, the circulating current cannot be suppressed satisfactorily.

Backstepping is a recursive Lyapunov-based scheme and often leads to better converter control performance [35]. It is more flexible and does not force linearity in the designed system [36,37], which is suitable for the systems that suffer from unknown disturbances. It has already been used in DC/DC systems [38,39] and a static VAR compensator (SVC) [40] to improve the performance of a single-converter control system. Although these achievements showed satisfactory tracking performance and acceptable adaptability to disturbances [41,42], they are not suitable for the plug-and-play parallel converter system in a four-port power switcher. On the one hand, a reliable circuiting current reduction strategy is needed to improve the system's efficiency and reliability; on the other hand, the control strategy must be designed based on accurate system parameters to ensure the balance of the parallel system. Consequently, a backstepping controller design for a converter is far from perfect. Based on the aforementioned considerations, this study aims to develop an adaptive backstepping control strategy with an online system parameter estimator for a parallel converter system in a four-port power switcher. The main contributions of this paper are as follows. First, an adaptive backstepping control strategy is proposed to manage the presence of unknown bounded disturbances, and the stability of the control system is proven using the Lyapunov function. By designing an adaptive law, the uncertainties caused by arbitrary plug and extraction processes are mitigated, and probability distributions are not needed. Second, the zero-component of the line current in the dq0 rotated coordinate system is controlled using a virtual control law to suppress the circulating current in the parallel structure, so the extra controller that is typical of circulating current

suppression is omitted. Moreover, the transient tracking performance control (TTPC) was designed by limiting the total errors of the voltage and current. Third, to further improve the system robustness, a parameter estimator based on the weighted least squares (WLS) was applied. In the estimator, no additional voltage and current sensors are needed, and the mean squared error (MSE) of the estimation can be minimized. Finally, simulation studies on a two-converter parallel system were performed in MATLAB/SIMULINK (R2018b, MathWorks, Natick, MA, USA) to verify the effectiveness of the adaptive backstepping control strategy.

The paper is organized as follows. In Section 2, the circulating current of the parallel structure is analyzed. In Section 3, the designs of the adaptive backstepping controller and the online parameter estimator (OPE) are described. Section 4 reports the simulation results to show the effectiveness of the proposed control method. Finally, Section 5 presents the conclusions.

2. Circulating Current Analysis

The main structure of the parallel system is shown in Figure 2. There are k converters in parallel that connect the common AC system and DC system. L_k, R_k, and C_k are the inductance, resistance, and capacitance of the k^{th} converter; i_{xk}, i_{xoutk}, and v_{cxk} are the inner current, output current, and output voltage of phase-x ($x = a, b, c$) in the k^{th} ($k = 1, 2, ..., n$) converter; u_{xk} is the voltage generated by the k^{th} converter; E_{sx} denotes the AC system voltage; i_{oxk} is the circulating current in the k^{th} converter.

As shown in Figure 2, the circulating current is generated by asynchronous switching operations and unbalanced system parameters in the same phase bridge arm of different converters. Actually, the circulating current in the k^{th} converter is the sum of the current caused by the other $k-1$ converters. Thus, it is a mathematical concept that cannot be detected by any sensors directly. In this paper, the circulating current is defined as the current only existing in the parallel structure; it can be found neither in the AC system, nor in the DC system. The mathematical definition is shown in Equation (1).

$$i_{oxk} = \frac{i_{sx}}{k} - i_{xoutk} \tag{1}$$

and the sum of the circulating current of phase-x in all k converters is zero, with:

$$\sum_{k=1}^{n} i_{oxk} = 0 \tag{2}$$

The frequency of circulating currents is the same in three phases of the k^{th} converter, and its frequency is equal to the fundamental frequency. It is well known that the zero-component in the dq0 coordinate system relates to the same components occurring in the three phases. Consequently, an extra circulating current suppression controller is not needed when designing the control strategy in the dq0 coordinate system and adding zero-component control.

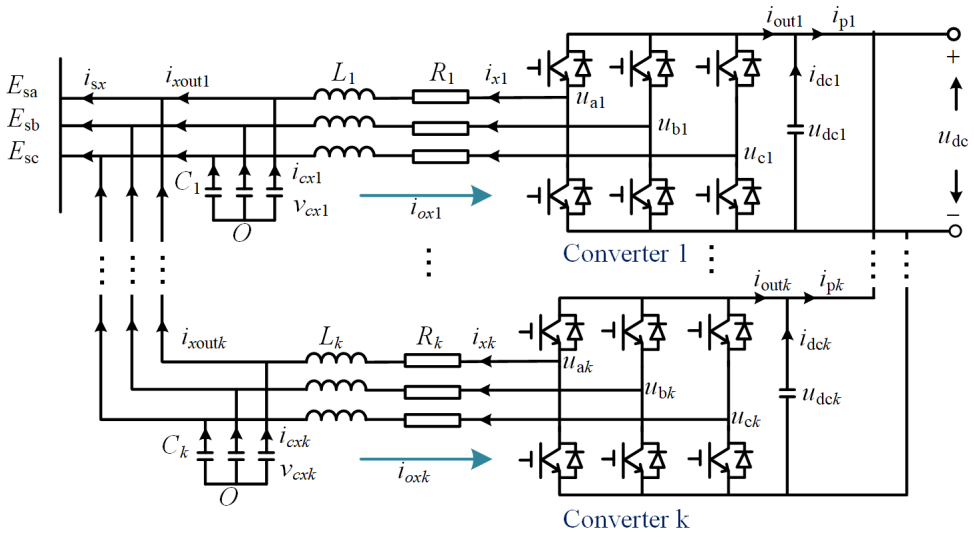

Figure 2. Circuit configuration of the parallel system.

3. System Model and Control Design

In order to eliminate the circulating current in the zero-component, the control strategy was designed in the dq0 coordinate system. First, the system model was built in the dq0 coordinate system; second, the backstepping controller was designed for the converter, and the stability of the system was verified using the Lyapunov function; third, the tracking errors were analyzed to optimize the dynamic performance; finally, an OPE was designed using a weighted least squares algorithm.

3.1. System Model

According to the converter system shown in Figure 2, the system states are defined as: $X_1 = [v_{cak} \quad v_{cbk} \quad v_{cck}]^T$, $X_2 = [i_{ak} \quad i_{bk} \quad i_{ck}]^T$, $U = [u_{ak} \quad u_{bk} \quad u_{ck}]^T$, $I = [i_{aoutk} \quad i_{boutk} \quad i_{coutk}]^T$. The dynamic model can be written in compact form as:

$$\begin{aligned} \dot{X}_1 &= G_1(I - X_2) \\ \dot{X}_2 &= F_1 U - F_2 X_2 - F_1 X_1 + \phi_2 \xi \end{aligned} \tag{3}$$

where ξ is the unknown bounded disturbances of the AC and DC buses caused by arbitrary plug and extraction operations; these are bounded external disturbances that are defined and controlled to guarantee system adaptivity and robustness. L and R denote the resistance and inductance, and:

$$F_1 = \begin{bmatrix} \frac{1}{L} & 0 & 0 \\ 0 & \frac{1}{L} & 0 \\ 0 & 0 & \frac{1}{L} \end{bmatrix}, G_1 = \begin{bmatrix} \frac{1}{C} & 0 & 0 \\ 0 & \frac{1}{C} & 0 \\ 0 & 0 & \frac{1}{C} \end{bmatrix}, F_2 = \begin{bmatrix} \frac{R}{L} & 0 & 0 \\ 0 & \frac{R}{L} & 0 \\ 0 & 0 & \frac{R}{L} \end{bmatrix}, \phi_2 = \begin{bmatrix} \frac{1}{L} \\ \frac{1}{L} \\ \frac{1}{L} \end{bmatrix} \tag{4}$$

The transformational matrix from the abc coordinate system applied to the dq0 coordinate system and the inverse transformation matrix in this paper are:

$$C_{\text{abc}-\text{dq0}} = \frac{2}{3} \begin{bmatrix} \cos\theta & \cos(\theta - 2\pi/3) & \cos(\theta + 2\pi/3) \\ \sin\theta & \sin(\theta - 2\pi/3) & \sin(\theta + 2\pi/3) \\ 1/2 & 1/2 & 1/2 \end{bmatrix} \tag{5}$$

$$C_{\text{dq0}-\text{abc}} = \begin{bmatrix} \cos\theta & \sin\theta & 1 \\ \cos(\theta - 2\pi/3) & \sin(\theta - 2\pi/3) & 1 \\ \cos(\theta + 2\pi/3) & \sin(\theta + 2\pi/3) & 1 \end{bmatrix} \tag{6}$$

Using Equations (3) and (5) and applying some mathematical manipulations, the dynamic model in the dq0 coordinate system can be expressed as:

$$\begin{aligned} \dot{X}_{1dq} =& G_1 I_{dq} - G_1 X_{2dq} - W X_{1dq} \\ \dot{X}_{2dq} =& F_1 u_{dq} - H X_{2dq} - F_1 X_{1dq} + M\xi \end{aligned} \tag{7}$$

where $H = \begin{bmatrix} \frac{R}{L} & -\omega & 0 \\ \omega & \frac{R}{L} & 0 \\ 0 & 0 & \frac{R}{L} \end{bmatrix}$, $W = \begin{bmatrix} 0 & -\omega & 0 \\ \omega & 0 & 0 \\ 0 & 0 & 0 \end{bmatrix}$, $M = C_{abc-dq0}\phi_2$, ω is the angular frequency, and $\omega = 2\pi f$ with f is the system frequency.

3.2. Backstepping Controller Design

A backstepping control strategy was adopted, and forcing the system states to track the desired reference commands requires two steps. The first step is to minimize the tracking error of the voltage X_1. The second step is to control the current X_2. Additionally, the update law of the unknown bounded disturbances is obtained by using the Lyapunov-based scheme.

The dynamic model of the system in consideration is shown in Equation (7), and the procedures of the backstepping controller design are as follows:

Step 1: Introducing the change in coordinates:

$$E_1 = X_{1dq} - X_{1dqref} = [v_{cdk}\, v_{cqk}\, v_{c0k}]^T - [v_{cdkref}\, v_{cqkref}\, v_{c0kref}]^T \tag{8}$$

$$E_2 = X_{2dq} - X_{2dqref} = [i_{dk}\, i_{qk}\, i_{0k}]^T - [i_{dkref}\, i_{qkref}\, i_{0kref}]^T \tag{9}$$

where X_{2dqref} is a virtual controller and X_{1dqref} is the reference signal. Equation (8) defines the tracking error control.

The derivative of Equation (8) is:

$$\dot{E}_1 = \dot{X}_{1dq} - \dot{X}_{1dqref} = G_1 I_{dq} - G_1 X_{2dq} - W X_{1dq} - \dot{X}_{1dqref} \tag{10}$$

The design of the stabilizing function X_{2dqref} is:

$$X_{2dqref} = G_1^{-1}(G_1 I_{dq} - W X_{1dq} - \dot{X}_{1dqref}) \tag{11}$$

According to Equations (10) and (11) and the definition of E_2, we get:

$$\dot{E}_1 = -G_1 E_2 \tag{12}$$

Step 2: We now consider the control variable in Equation (9). The derivative of E_2 is:

$$\begin{aligned} \dot{E}_2 =& \dot{X}_{2dq} - \dot{X}_{2dqref} \\ =& F_1 u_{dq} - H X_{2dq} - F_1 X_{1dq} + M\xi \\ & - \frac{\partial X_{2dqref}}{\partial X_{1dq}} \left[G_1 I_{dq} - G_1 X_{2dq} - W X_{1dq} \right] - \frac{\partial X_{2dqref}}{\partial \dot{X}_{1dqref}} \ddot{X}_{1dqref} \end{aligned} \tag{13}$$

In this equation, the actual control input u_{dq} is at our disposal. The control law can be designed as:

$$\begin{aligned} u_{dq} =& F_1^{-1}[H X_{2dq} + F_1 X_{1dq} - M\hat{\xi} + \frac{\partial X_{2dqref}}{\partial X_{1dq}}(G_1 I_{dq} - G_1 X_{2dq} - W X_{1dq}) \\ & + \frac{\partial X_{2dqref}}{\partial \dot{X}_{1dqref}} \ddot{X}_{1dqref} + KE] \end{aligned} \tag{14}$$

where $\tilde{\xi} = \xi - \hat{\xi}$, $\hat{\xi}$ is the estimated value of ξ, and $E = [E_1, E_2]^T$, $K = [k_1 G_1^{-1}, -K_2]$, $K_2 = \begin{bmatrix} k_{11} & 0 & 0 \\ 0 & k_{22} & 0 \\ 0 & 0 & k_{33} \end{bmatrix}$, $k_1 > 0$, $k_{ii} > 0$, $i = 1,2,3$ are control parameters. Putting Equation (14) into Equation (13) yields:

$$\dot{E}_2 = KE + M\tilde{\xi} \tag{15}$$

The new error system can be represented as:

$$\begin{aligned} \dot{E}_1 &= -G_1 E_2 \\ \dot{E}_2 &= KE + M\tilde{\xi} \end{aligned} \tag{16}$$

Equation (16) can be rewritten in compact form as:

$$\dot{E} = AE + \phi\tilde{\xi} \tag{17}$$

where $A = \begin{bmatrix} \mathbf{0} & -G_1 \\ k_1 G_1^{-1} & -K_2 \end{bmatrix}$, $\phi = \begin{bmatrix} \mathbf{0} \\ M \end{bmatrix}$. The characteristic equation of the system shown in Equation (17) is:

$$|sI - A| = \begin{bmatrix} sI & G_1 \\ -k_1 G_1^{-1} & sI + K_2 \end{bmatrix} = Is^2 + K_2 s + k_1 I = 0 \tag{18}$$

All the roots of the characteristic equation (Equation (18)) have a negative real part, so the coefficient matrix A of the system is a Hurwitz matrix, and the system has asymptotic stability. The positive-definite matrices P and $Q = \begin{bmatrix} 1 & 0 & 0 \\ 0 & 1 & 0 \\ 0 & 0 & 1 \end{bmatrix}$ satisfy:

$$A^T P + PA = -Q \tag{19}$$

The task in this step is to stabilize the (E_1, E_2)-system in Equation (17) with respect to:

$$V = \frac{1}{2} E^T P E + \frac{1}{2\gamma}\tilde{\xi}^2 \tag{20}$$

where γ is a positive constant. The derivative of V is:

$$\begin{aligned} \dot{V} =& \frac{1}{2}(\dot{E}^T P E + E^T P \dot{E}) + \frac{1}{\gamma}\tilde{\xi}\dot{\tilde{\xi}} \\ =& \frac{1}{2} E^T (A^T P + PA) E + (\frac{1}{2} E^T P \phi + \frac{1}{2}\phi^T P E - \frac{1}{\gamma}\dot{\hat{\xi}})\tilde{\xi} \\ =& -\frac{1}{2} E^T Q E + (\frac{1}{2} E^T P \phi + \frac{1}{2}\phi^T P E - \frac{1}{\gamma}\dot{\hat{\xi}})\tilde{\xi} \end{aligned} \tag{21}$$

Now, we select the update law of the unknown bounded disturbance $\dot{\hat{\xi}}$, where:

$$\dot{\hat{\xi}} = \frac{1}{2}\gamma(E^T P \phi + \phi^T P E) \tag{22}$$

The resulting derivative of V can be written as:

$$\dot{V} = -\frac{1}{2} E^T Q E < 0, \ \forall E \neq 0 \tag{23}$$

By using the control law in Equation (14) and the unknown disturbance update law in Equation (22), the converter system in Equation (7) has asymptotic stability at the equilibrium

point $E = 0$. It follows that $E_1, E_2 \to 0$, and this further implies that $lim_{t\to\infty}(X_{1\mathrm{dq}} - X_{1\mathrm{dqref}}) = 0$. As backstepping achieves the goals of stabilization and tracking, the final control law in the dq0 coordinate system can be obtained by substituting $F_1, H, \phi_2, G_1, W, K$, and E into Equation (14).

3.3. Transient Tracking Performance Control

The system is globally stable in the sense that all signals in the closed loop are bounded. From the stable filter dynamics and minimum phase condition, we can conclude that all the signals are bounded. It can be determined that:

$$\begin{cases} E_1 \to 0 & \text{as} \quad \mathrm{t} \to \infty \\ E_2 \to 0 & \text{as} \quad \mathrm{t} \to \infty \end{cases} \tag{24}$$

That is to say,

$$\begin{cases} \lim_{t\to\infty} X_{1\mathrm{dq}} - X_{1\mathrm{dqref}} = 0 \\ \lim_{t\to\infty} X_{2\mathrm{dq}} - X_{2\mathrm{dqref}} = 0 \end{cases} \tag{25}$$

Since V is non-increasing, we have:

$$\|E(t)\|_2^2 = \int_0^\infty E(t)^T E(t) dt \le \int_0^\infty -2\dot{V} dt = 2(V(0) - V(\infty)) \le 2V(0) \tag{26}$$

The initial value of V can be calculated as:

$$V(0) = \frac{1}{2} E(0)^T P E(0) + \frac{1}{2\gamma} \tilde{\xi}(0)^2 \tag{27}$$

Thus, the transient tracking error performance is given by:

$$\|E(t)\|_2 \le \left(\frac{1}{2} E(0)^T P E(0) + \frac{1}{2\gamma} \tilde{\xi}(0)^2 \right)^{1/2} \tag{28}$$

The transient performance depends on the initial estimate errors and the explicit design parameters.

3.4. Online Parameter Estimator Design

Rewriting the second equation in Equation (3) and ignoring the unknown bounded disturbances ξ, we have:

$$L \frac{di_{xk}}{dt} = u_{xk} - R i_{xk} - v_{cxk} \tag{29}$$

with:

$$u_{xk} = \left(s_k - \frac{1}{3} \sum_{j=\mathrm{a,b,c}} s_j \right) u_{dck} \tag{30}$$

where s_k denotes the switching function.

Defining $y = i_{xk}$ and $z = u_{xk} - v_{cxk}$, Equation (29) can then be expressed as:

$$\frac{dy}{dt} = -\frac{R}{L} y + \frac{1}{L} z \tag{31}$$

Filtering each side of Equation (31) with $1/(s + \lambda_\mathrm{f})$, where λ_f is a selected positive real constant, we then have:

$$y = y_\mathrm{f}(\lambda_\mathrm{f} - h_1) - z_\mathrm{f} h_2 \tag{32}$$

where $h_{RL} = R/L$, $h_L = 1/L$, $y_\mathrm{f} = \dfrac{y}{s+\lambda_\mathrm{f}}$, and $z_\mathrm{f} = \dfrac{z}{s+\lambda_\mathrm{f}}$.

Expressing Equation (32) as:

$$y = Ph \tag{33}$$

where $P = [y_\mathrm{f} \quad z_\mathrm{f}] = [\rho_\mathrm{a} \quad \rho_\mathrm{b}]$, $h = [\lambda_\mathrm{f} - h_{RL} \quad h_L]^T = [h_\mathrm{a} \quad h_\mathrm{b}]^T$, and h denotes the true parameter values related to R and L.

The parameter estimation problem turns into a linear weighted least squares (WLS) problem, where the objective is to estimate vector h from m linear observations y. The system can be expressed as:

$$y_i = P_i h \quad i = 1, 2, ..., m \tag{34}$$

The above can be rewritten in compact form as:

$$y^m = P^m h \tag{35}$$

where:

$$\begin{aligned} y^m &= [y_1^T \quad y_2^T \quad \dots \quad y_m^T]^T \\ P^m &= [P_1^T \quad P_2^T \quad \dots \quad P_m^T]^T \end{aligned} \tag{36}$$

such that the fitting error is minimized by:

$$J_m = (y_m - P^m h)^T \Gamma^m (y_m - P^m h) \tag{37}$$

where $\Gamma^m = \mathrm{diag}\{\gamma_1, \gamma_2, \dots, \gamma_m\}$.

The WLS estimator that minimizes the above is obtained by setting its gradient to zero with regard to h:

$$\begin{aligned} \nabla_h J_m &= \begin{bmatrix} \dfrac{\partial}{\partial h_\mathrm{a}} \\ \dfrac{\partial}{\partial h_\mathrm{b}} \end{bmatrix} J_m = \begin{bmatrix} -2\sum_{i=1}^m \gamma_i (y_i - \sum_{j=\mathrm{a,b}} \rho_{ij} h_j) \rho_{i\mathrm{a}}) \\ -2\sum_{i=1}^m \gamma_i (y_i - \sum_{j=\mathrm{a,b}} \rho_{ij} h_j) \rho_{i\mathrm{b}}) \end{bmatrix} \\ &= -2(P^m)^T \Gamma^m (y^m - P^m h) = 0 \end{aligned} \tag{38}$$

The estimation of h by using m historical datasets can be calculated, which yields:

$$\hat{h}_m^{WLS} = ((P^m)^T \Gamma^m P^m)^{-1} (P^m)^T \Gamma^m y^m \tag{39}$$

It can be easily seen that since Γ^m is positive-definite, the Hessian of J_m with regard to h is positive-definite. Consequently, the extreme point $\hat{h}_m$ is a minimum.

3.5. Block Diagram of the Proposed Control Strategy

The block diagram of the adaptive backstepping control method with an OPE for a plug-and-play two-converter parallel system in a four-port power switcher is shown in Figure 3. In the figure, PLL denotes the phase-locked loop, PWM denotes pulse width modulation, and abc/dq0 and dq0/abc denote the dq transformation and inverse transformation shown in Equations (5) and (6), respectively.

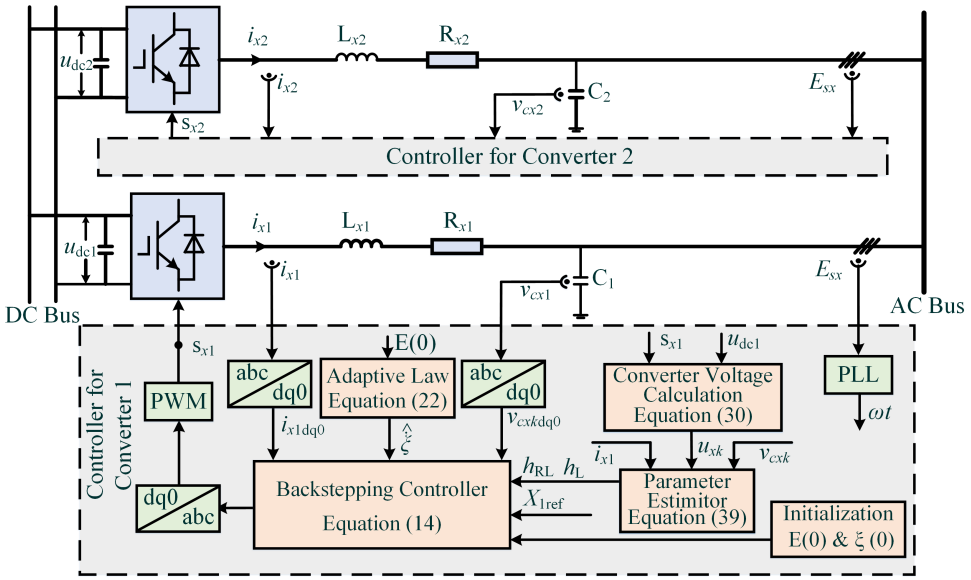

Figure 3. Block diagram of the adaptive backstepping control strategy with an OPE for a two-converter system.

4. Simulation Study

To verify the effectiveness of the proposed control strategy, simulation studies were conducted on a single converter and a two-converter parallel system in MATLAB/SIMULINK, respectively.

The main parameters of the system and controller are listed in Table 1. In the OPE, two historical datasets were used. The matrix Γ^m is defined as $\Gamma^2 = \text{diag}\{\ \gamma_1, \gamma_2\ \}$. The parameters of the IGBT (Insulated Gate Bipolar Transistor) are shown in Table 2.

Table 1. Main parameters of the system and controller.

Parameters	Value
AC voltage/V	380
DC voltage/V	±380
L_k/mH	12
R_k/Ω	5
k_1	1×10^{15}
k_{11}, k_{12}, k_{13}	1×10^{10}
γ_1	5000
γ_2	2500

Table 2. Parameters of IGBT.

Parameters	Value
Number of bridge arms	3
Snubber resistance/Ω	1×10^5
Snubber capacitance/F	infinity
Internal resistance/Ω	1×10^{-3}
Forward voltage of IGBT/V	1
Forward voltage of antiparallel diodes/V	1.2

In order to show the transient tracking performance of the controller, a single-converter system was built. The voltage references were selected, which are shown in Figure 4. Figure 4a–d show the corresponding references for the different step changes: amplitude, phase, frequency, and all three

together, respectively. Initially, the amplitude (phase, frequency) of voltage reference X_{1ref} is 55 V (15°, 49 Hz). At 0.02 s, it steps up to 65 V (30°, 50 Hz). At 0.04 s, the reference reverts to the initial state.

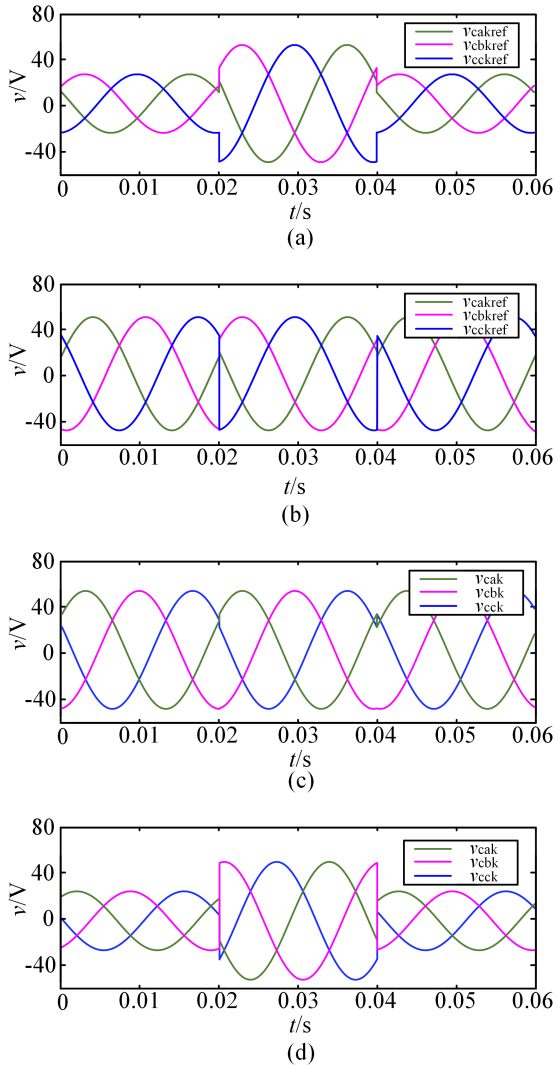

Figure 4. Voltage reference: (**a**) v_{cxkref}, amplitude step changes; (**b**) v_{cxkref}, phase step changes; (**c**) v_{cxkref}, frequency step changes; (**d**) v_{cxkref}, amplitude, phase, and frequency step changes simultaneously.

In Figure 5, the responses of the converter to tracking the reference in Figure 4 are shown. From Figure 5, it can be seen that by using the designed backstepping controller, the voltage follows the reference for a finite duration of time, and the settling time of both results is short. However, the performance is affected by the TTPC.

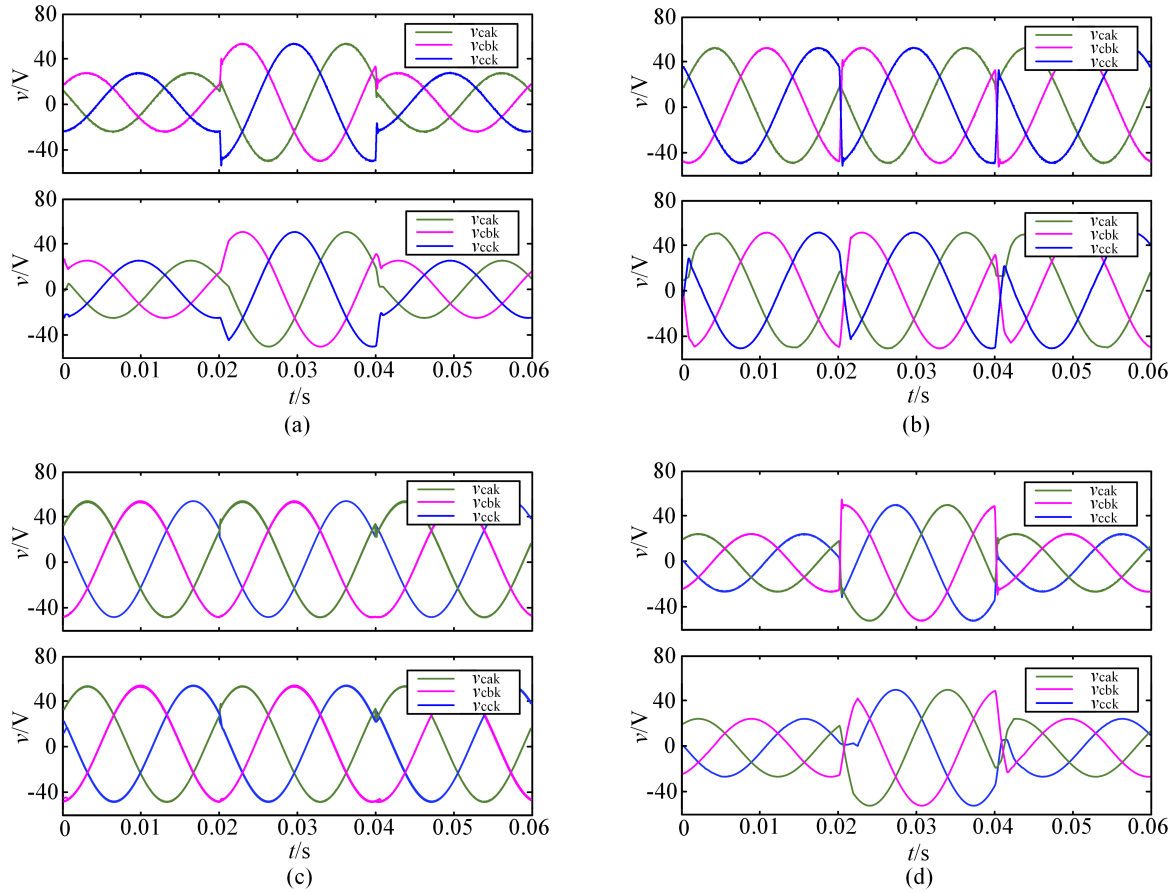

Figure 5. Voltage v_{cxk} transient tracking performance: (**a**) with (upper) and without transient tracking performance control (TTPC) for amplitude step changes; (**b**) with (upper) and without TTPC for phase step changes; (**c**) with (upper) and without TTPC for frequency step changes; (**d**) with (upper) and without TTPC for amplitude, phase, and frequency step changes simultaneously.

The details of the transient performance at $t = 0.04$ s are shown in Figure 6. The settling times of different conditions are as follows: 0.0003 s (upper) and 0.001 s for (a), 0.0002 s (upper) and 0.0027 s for (b), 0.0005 s (upper) and 0.0012 s for (c), and 0.0005 s (upper) and 0.0025 s for (d). In order to further analyze the transient tracking performance directly, the total error that occurs during the dynamic process is defined as:

$$e_{sum} = \sum_{t=0.04}^{0.045} \sum_{x=\mathrm{a,b,c}} \|v_{cx1ref} - v_{cx1}\|^2 \tag{40}$$

With a 50-kHz sample frequency, there are 250 sample data points during t = 0.04 s∼0.045 s. According to Figure 6, the total error from $t = 0.04$ s to $t = 0.045$ s is: 5.183 $\times 10^3$ (upper) and 2.034 $\times 10^4$ for (a), 8.280 $\times 10^4$ (upper) and 1.473 $\times 10^5$ for (b), 5.267 $\times 10^3$ (upper) and 1.476 $\times 10^4$ for (c), and 6.093 $\times 10^4$ (upper) and 1.100 $\times 10^5$ for (d). Obviously, the TTPC algorithm results in better dynamic performance.

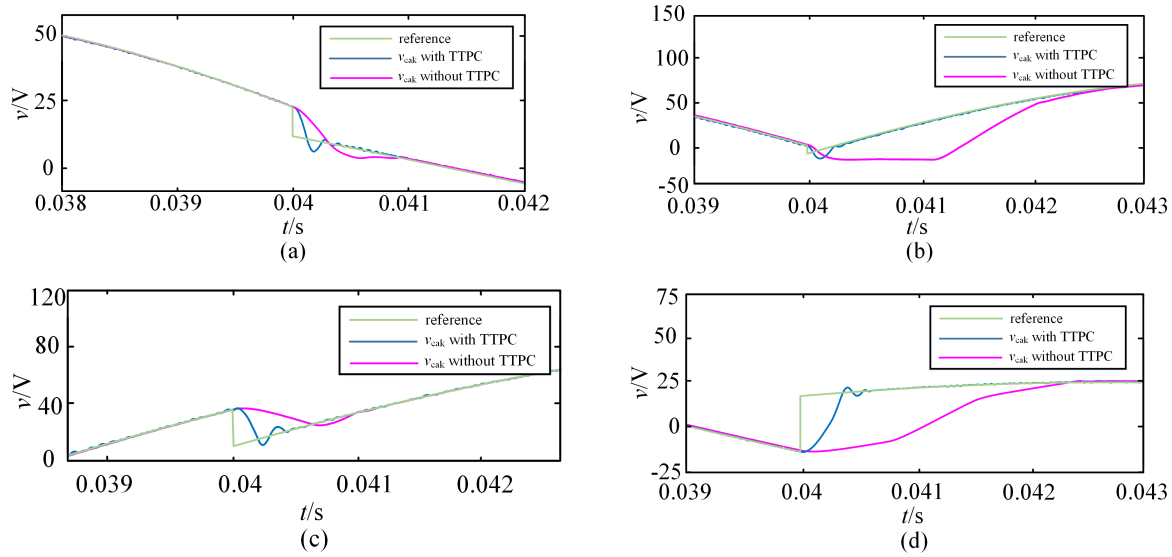

Figure 6. Detail of voltage v_{cxk} transient tracking performance at $t = 0.04$ s: (**a**) with and without TTPC for amplitude step changes; (**b**) with and without TTPC for phase step changes; (**c**) with and without TTPC for frequency step changes; (**d**) with and without TTPC for amplitude, phase, and frequency step changes simultaneously.

From Figure 7, we can observe the circuiting currents of Phase a in the two-converter parallel system for Converter 1 (a) and Converter 2 (b). The circuiting currents in three phases of one converter are the same, $i_{oa1} = i_{ob1} = i_{oc1}$ and $i_{oa2} = i_{ob2} = i_{oc2}$. Furthermore, the circuiting currents are opposite in Converter 1 and Converter 2, which demonstrates the correctness of Equation (2).

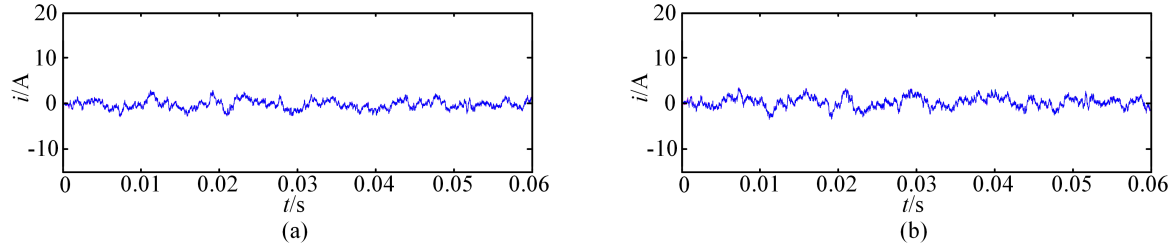

Figure 7. Circuiting current of a two-converter parallel system: (**a**) i_{oa1}; (**b**) i_{oa2}.

The comparison of circuiting current control performances can be seen in Figure 8. In this simulation, the inductance and resistance of Converter 2 are 5% larger than those of Converter 1. Unbalanced parameters will arise in larger circuiting currents. From Figure 8, we can see that by using zero-component control, the circulating current decreases significantly. The amplitude of circuiting currents is reduced by 60% compared with the results without zero-component control.

The dynamic processes of current and active and reactive power for the plug-and-play operation are shown in Figures 9 and 10, respectively. Initially, only Converter 1 is switched on. At 0.02 s, both converters are switched on. At 0.04 s, it reverts to the initial state. In Figure 9a,b, the current with and without the OPE is shown. It is obvious that the distribution of the current is similar in (a) and (b). The current of Converter 1 is 80 A when only one converter is switched on, and the current is 40 A when two converters are switched on. Thus, the current is balanced between the two converters. However, there is better power quality with the OPE. The total harmonic distortion (THD) during t = 0.02 s~0.04 s is 2.04% and 13.09%, respectively. Moreover, the settling time at $t = 0.04$ s is reduced by 90%.

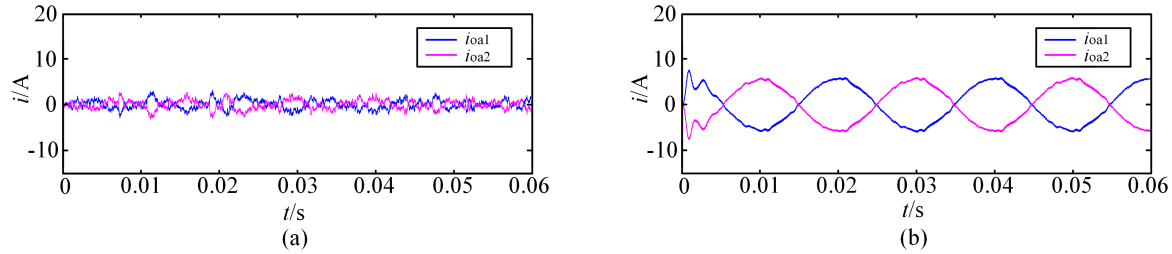

Figure 8. Circuiting current in Phase a i_{oak} of a two-converter parallel system: (**a**) with zero-component control; (**b**) without zero-component control.

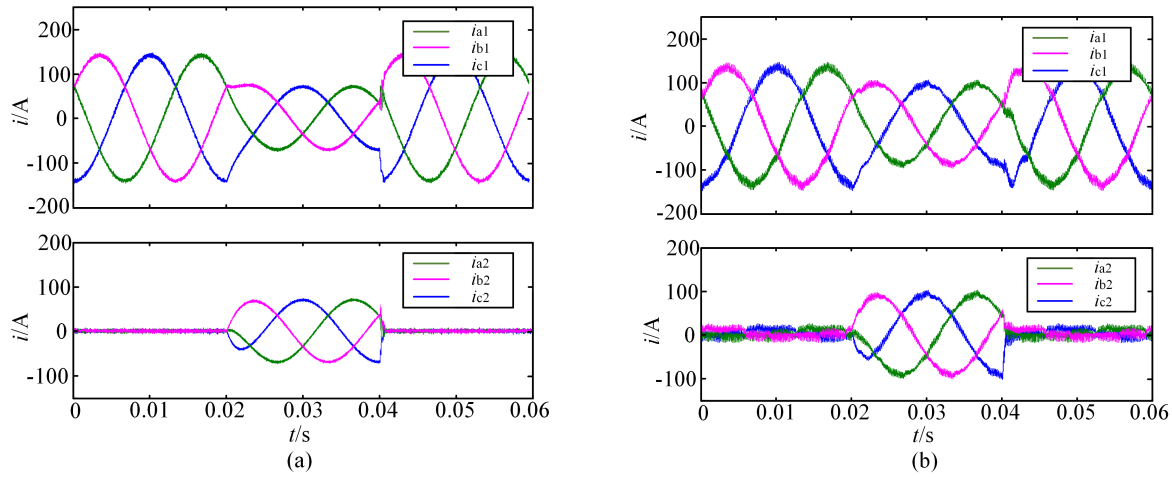

Figure 9. Dynamic process of plug-and-play: (**a**) i_{x1}, current of Converters 1 and 2 with the online parameter estimator (OPE); (**b**) i_{x1}, current of Converters 1 and 2 without the OPE.

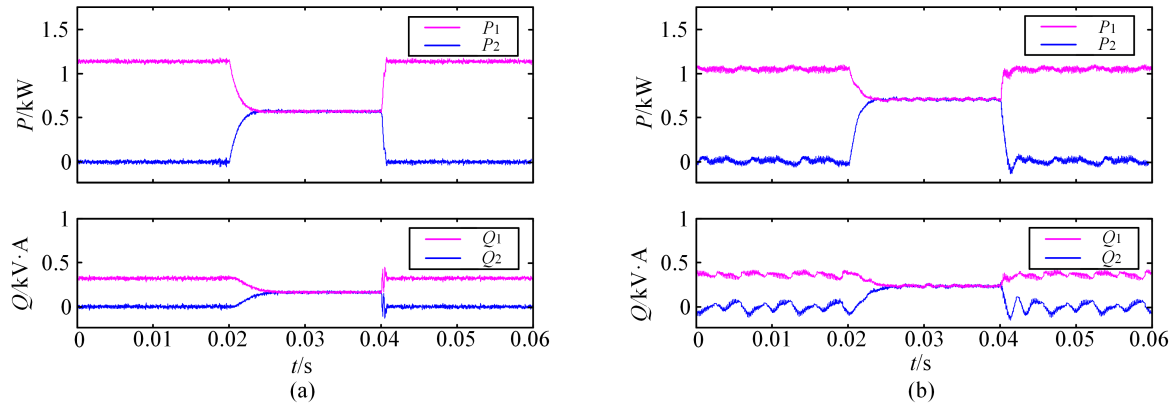

Figure 10. Dynamic process of plug-and-play: (**a**) active and reactive power with the OPE; (**b**) active and reactive power without the OPE.

Similarly, in Figure 10a,b, the active power and reactive power with and without the OPE for the plug-and-play operation are shown. It can be observed that the active power and reactive power are balanced between the two converters, and the power ripples are fully eliminated with the OPE.

The adaptation for the unknown disturbance ξ is verified in Figure 11. Initially, the unknown disturbance is 5% of the DC voltage. At 0.02 s, it increases to 50%. At 0.04 s, it reverts to the initial state. The responses of active power and reactive power, $v_{cx}1$ and i_{x1}, respectively, are shown. Obviously, by using the update law in Equation (22), the influence of the unknown disturbances is reduced effectively. Even suffering from a 50% disturbance, an acceptable performance is achieved in (a). In addition, the total harmonic distortion (THD) from $t = 0$ s to $t = 0.02$ s is 0.27% and 2.80% for

voltage and current when using the update law in Equation (22), while it is 3.51% and 7.52% for voltage and current when not using the update law. Similarly, the THD from $t = 0.02$ s to $t = 0.04$ s is 1.46% and 5.85% for voltage and current when using the update law in Equation (22), while it is 9.35% and 11.49% for voltage and current when not using the update law.

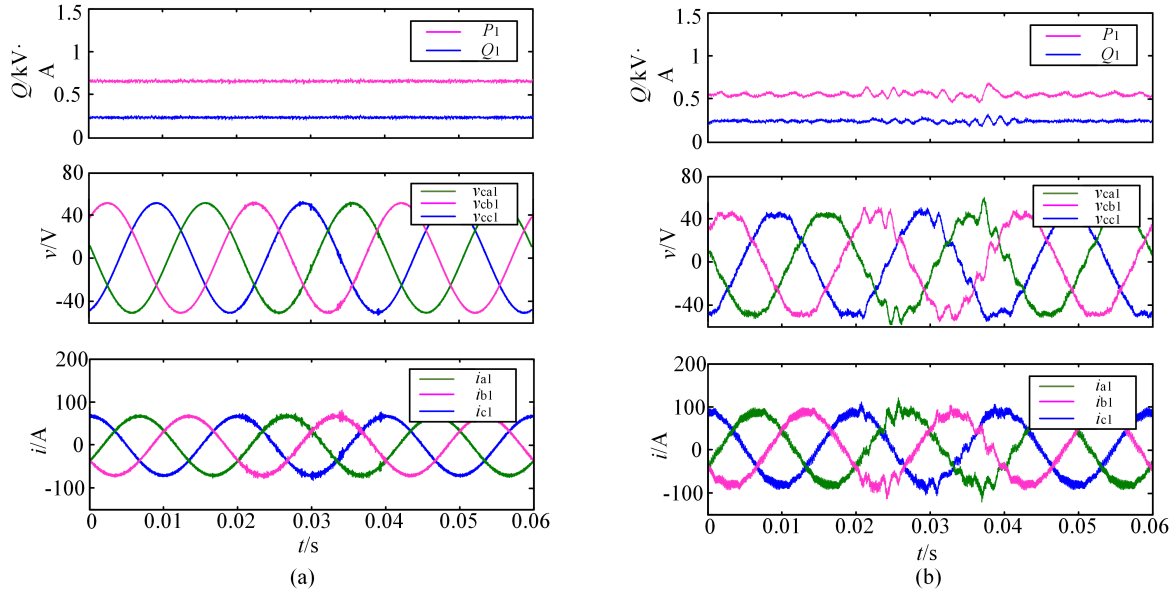

Figure 11. Responses of Converter 1 with unknown bounded disturbances in the DC system: (**a**) responses with bounded disturbance adaptation control; (**b**) responses without bounded disturbance adaptation control.

5. Conclusions

This paper presents an adaptive backstepping control strategy with an OPE to manage the obstacles that arise when using a plug-and-play parallel converter structure in a four-port power switcher. The main conclusions are as follows. First, the adoption of the adaptive backstepping control strategy increases the robustness and guarantees the closed-loop stability of the system. Moreover, transient tracking performance is controlled by limiting the maximum total errors to achieve better transient performance. Second, by adding the zero-component to the conventional dq-based control process, the circulating currents in the parallel structure are fully eliminated. Additionally, an OPE is implemented by solving a WLS problem to guarantee the reliability of the control strategy. The proposed scheme is capable of ensuring the performance of tracking errors and the global stability of the overall closed-loop system for the plug-and-play function. Theoretical analysis and simulation studies in MATLAB/SIMULINK verify the effectiveness of the proposed adaptive backstepping control strategy.

Author Contributions: C.G. conceived of and performed the research; H.Z. designed parameters of the model; C.G. and A.Z. wrote the paper; L.Z. revised the manuscript. All of the authors were involved in preparing this manuscript.

Funding: This research was funded by the National Natural Science Foundation of China, Grant Number 51607133.

Conflicts of Interest: The authors declare no conflict of interest.

References

1. Wanxing, S.; Qing, D.; Xiaoli, M.; Haitao, L.; Changkai, S. Research on the AC & DC seamless-hybrid fluent power distribution system following the power electronics evolution. *Proc. CSEE* **2017**, *37*, 1877–1888. [CrossRef]
2. Iyer, A.R.; Kandula, R.P.; Moghe, R.; Hernandez, J.E.; Lambert, F.C.; Divan, D. Validation of the plug-and-play ac/ac power electronics building block (AC-PEBB) for medium-voltage grid control applications. *IEEE Trans. Ind. Appl.* **2014**, *50*, 3549–3557. [CrossRef]
3. Mohammad, M.; Parisa, M.S.; Ali, M. Analysis and output voltage control of a high-efficiency converter for DC microgrids. In Proceedings of the IEEE Conference on Industrial Electronics Society, Washington, DC, USA, 21–23 October 2018.
4. Rifkin, J. *Third Industrial Revolution: How Lateral Power Is Transforming Energy, the Economy, and the World*; Palgrave Macmillan: New York, NY, USA, 2011; pp. 31–46.
5. Ghaffarianfar, M.; Hajizadeh, A. Voltage stability of low-voltage distribution grid with high penetration of photovoltaic power units. *Energies* **2018**, *11*, 1960. [CrossRef]
6. Ashabani, M.; Mohamed, I.; Mirsalim, M.; Aghashabani, M. Multivariable droop control of synchronous current converters in weak grids/micro-grids with decoupled dq-axes currents. *IEEE Trans. Smart Grid* **2015**, *6*, 1610–1620. [CrossRef]
7. Xia, Y.; Wei, W.; Peng, Y.; Yang, P.; Yu, M. Decentralized coordination control for parallel bidirectional power converters in a grid-connected dc micro-grid. *IEEE Trans. Smart Grid* **2017**. [CrossRef]
8. Yang, J.; Cui, H.; Li, S.; Zolotas, A. Optimized active disturbance rejection control for DC-DC buck converters with uncertainties using a reduced-order GPI observer. *IEEE Trans. Circuits Syst. I Regul. Pap.* **2018**, *65*, 832–841. [CrossRef]
9. Feng, G.; Huang, L.; Zhu, D. High performance control of induction motor based on auto-disturbance rejection controller. *Proc. CSEE* **2001**, *21*, 55–58. [CrossRef]
10. Song, J.; Gan, Z.; Han, J. Study of active disturbance rejection controller on filtering. *Control Decis.* **2003**, *18*, 55–58. [CrossRef]
11. Wang, B.; Shen, Z.; Liu, H.; Hu, J. Linear ADRC direct current control of grid-connected inverter with LCL filter for both active damping and grid voltage induced current distortion suppression. *IET Power Electron.* **2018**, *11*, 1748–1755. [CrossRef]
12. Yang, N.; Gao, F.; Paire, D.; Miraoui, A.; Liu, W. Distributed control of multi-time scale DC micro-grid based on ADRC. *IET Power Electron.* **2017**, *10*, 329–337. [CrossRef]
13. Wang, J.; Li, S.; Yang, J.; Wu, B.; Li, Q. Extended state observer-based sliding mode control for PWM-based DC–DC buck power converter systems with mismatched disturbances. *IET Control Theory Appl.* **2014**, *9*, 579–586. [CrossRef]
14. Zhang, D.; Yao, X,; Wu, Q.; Song, Z. ADRC based control for a class of input time delay systems. *J. Syst. Eng. Electron.* **2017**, *28*, 1210–1220. [CrossRef]
15. Xue, W.; Bai, W.; Yang, S.; Song, K.; Huang, Y.; Xie, H. ADRC with adaptive extended state observer and its application to air-fuel ratio control in gasoline engines. *IEEE Trans. Ind. Electron.* **2015**, *62*, 5847–5857. [CrossRef]
16. Lia, Y.; You, J.; Yang, J.; Wang, Z.; Jin, L. Disturbance-observer-based model predictive control for battery energy storage system modular multilevel converters. *Energies* **2018**, *11*, 2285. [CrossRef]
17. Yang, W.; Zhang, H.; Li, J.; Zhang, A.; Zhou, Y.; Wang, J. PIDR sliding mode current control with online inductance estimator for VSC-MVDC system converter stations under unbalanced grid voltage conditions. *Energies* **2018**, *11*, 2599. [CrossRef]
18. Yan, S.; Zhang, A.; Zhang, H.; Wang, J.; Cai, B. Optimized and coordinated model predictive control scheme for DFIGs with dc-based converter system. *J. Mod. Power Syst. Clean Energy* **2017**, *5*, 620–630. [CrossRef]
19. Vazquez, S.; Leon, J.I.; Franquelo, L.G.;Rodriguez, J.; Young, H.A.; Marquez, A.; Zanchetta, P. Model predictive control: A review of its applications in power electronics. *IEEE Ind. Electron. Mag.* **2014**, *8*, 16–31. [CrossRef]
20. Guo, C.J.; Zhang, A.M.; Zhang, H.; Ren, Z.G.; Zhang, L. A model predictive control method for bidirectional interfacing converters in hybrid ac/dc micro-grids. *J. Xi'an Jiaotong Univ.* **2018**, *52*, 40–46. [CrossRef]

21. Ramírez, R.O.; Espinoza, J.R.; Melín, P.E.; Reyes, M.E.; Espinosa, E.E.; Silva, C.; Maurelia, E. Predictive controller for a three-phase/single-phase voltage source converter cell. *IEEE Tran. Ind. Inform.* **2014**, *10*, 1878–1889. [CrossRef]
22. An, F.; Song, W.; Yang, K.; Hou, N.; Ma, J. Improved dynamic performanceof dual active bridge dc-dc converters using MPC scheme. *IET Power Electron.* **2018**, *11*, 1756–1765. [CrossRef]
23. Hooman, G.; Ali, M. Predictive set point modulation technique to enhance the dynamic response of a power system. In Proceedings of the IEEE Applied Power Electronics Conference and Exposition, Tampa, FL, USA, 26–30 March 2017; pp. 1134–1140. [CrossRef]
24. Young, H.A.; Perez, M.A.; Rodriguez, J. Analysis of finite-control-set model predictive current control with model parameter mismatch in a three-phase inverter. *IEEE Trans. Ind. Electron.* **2016**, *63*, 3100–3107. [CrossRef]
25. Mohammad, G.; Saeed, L. Control of flywheel energy storage systems in presence of uncertainties. *IEEE Trans. Sustain. Energy* **2018**. [CrossRef]
26. Zhang, Y.; Kang, Y.; Chen, J. The zero-sequence circulating currents between parallel three-phase inverters with three-pole transformers and reactors. In Proceedings of the IEEE Applied Power Electronics Conference and Exposition, Dallas, TX, USA, 19–23 March 2006; pp. 1710–1715. [CrossRef]
27. Sun, X.; Wong, L.; Lee, Y.; Xu, D. Design and analysis of an optimal controller for parallel multi-inverter systems. *IEEE Trans. Circuits Syst. II Express Briefs* **2006**, *53*, 56–61. [CrossRef]
28. Lia, Y.; Chen, H.C. Simplified PWM with switching constraint method to prevent circulating currents for paralleled bidirectional AC/DC converters in grid-tied system using graphic analysis. *IEEE Trans. Ind. Electron.* **2015**, *62*, 4573–4586. [CrossRef]
29. Zhang, X.; Chen, J.; Ma, Y.; Wang, Y.; Xu, D. Bandwidth expansion method for circulating current control in parallel three-phase PWM converter connection system. *IEEE Trans. Power Electron.* **2014**, *29*, 6847–6856. [CrossRef]
30. Zhang, X.; Zhang, W.; Chen, J.; Xu, D. Deadbeat control strategy of circulating currents in parallel connection system of three-phase PWM converter. *IEEE Trans. Energy Convers.* **2014**, *29*, 406–417. [CrossRef]
31. Zhang, Y.; Yu, M.; Liu, F.; Li, S.; Wang, J.; Kang, Y. Instantaneous current share method for modular UPS through virtual impedance. In Proceedings of the IEEE Conference on Industrial Electronics Society, Melbourne, Australia, 7–10 November 2011; pp. 1384–1389. [CrossRef]
32. Sun, B.; Liu, H.; Wu, H.; Wang, W. A suppression method of circulating current in parallel photovoltaic system based on virtual impedance. In Proceedings of the IEEE Conference on International Power Electronics and Motion Control, Hefei, China, 22–26 May 2016; pp. 1532–1538. [CrossRef]
33. Shi, H.; Zhuo, F.; Zhang, D.; Geng, Z.; Wang, F. Adaptive implementation strategy of virtual impedance for paralleled inverters UPS. In Proceedings of the IEEE Energy Conversion Congress and Exposition, Pittsburgh, PA, USA, 14–18 September 2014; pp. 158–162. [CrossRef]
34. Cai, J.; Chen, C.; Liu, P.; Duan, S. Adaptive current-sharing control strategy with virtual circulating impedance for parallel operation of UPS. In Proceedings of the IEEE Energy Conversion Congress and Exposition, Montreal, QC, Canada, 22–24 September 2015; pp. 1243–1247. [CrossRef]
35. Sureshkumar, R,; Ganeshkumar, S. Comparative study of proportional integral and backstepping controller for buck converter. In Proceedings of the International Conference on Emerging Trends in Electrical and Computer Technology, Nagercoil, India, 23–24 March 2011; pp. 375–379. [CrossRef]
36. Song, Z.; Sun, K. Adaptive backstepping sliding mode control with fuzzy monitoring strategy for a kind of mechanical system. *ISA Trans.* **2014**, *53*, 125–133. [CrossRef] [PubMed]
37. Zhang, L.; Zhang, A.; Han, J.; Zhang, H. Adaptive backstepping passivity feedback control design of static volt-ampere reactive compensator. *Control Theory Appl.* **2012**, *29*, 298–304. [CrossRef]
38. Yuz, A.; Diego, L.; Jesus, L.; Luis, H.; Victor, M. Adaptive backstepping control for a fuel cell/boost converter system. *IEEE J. Emerg. Sel. Top. Power Electron.* **2018**, *6*, 686–695. [CrossRef]
39. Mahdi, S.; Jafar, S.; Gholamreza, A.; Navid, R. Indirect output voltage regulation of dc-dc buck/boost converter operating in continuous and discontinuous conduction modes using adaptive backstepping approach. *IET Power Electron.* **2012**, *6*, 732–741. [CrossRef]
40. Su, Q.; Dong, F.; Shen, X. Improved adaptive backstepping sliding mode control of static var compensator. *Energies* **2018**, *11*, 2750. [CrossRef]

41. Sun, D.; Wang, X.; Yang, F. Backstepping direct power control without phase-locked loop of AC/DC converter under both balanced and unbalanced grid conditions. *IET Power Electron.* **2016**, *9*, 1614–1624. [CrossRef]
42. Wang, G.; Wai, R.; Liao, Y. Design of backstepping power control for grid-side converter of voltage source converter-based high-voltage dc wind power generation system. *IET Renew. Power Gen.* **2012**, *7*, 118–133. [CrossRef]